Gas-Phase Micro-Solvation within Zeolite Confinement Accelerates Hydrogen Isotope Exchange

Hongbing Wang[a*], *Yilin Liao*[a], *Jiaju Tang*[a], *Shuai Liu*[a], *Xiangdong Zeng*[a], Wei Cui[b]

[a] College of Materials and Chemistry & Chemical Engineering, Chengdu University of Technology, Chengdu, 610059, China.

[b] School of Chemical Sciences, University of Chinese Academy of Sciences, Beijing 100049, China.

Experimental section

Catalyst Synthesis and Preparation

The zeolite-encapsulated Pt catalysts (denoted as Pt@zeolite) were synthesized via a modified procedure based on a previous report[1]. The overall synthetic procedure is schematically illustrated in Scheme 1. Initially, amorphous silica-coated Pt nanoparticles (Pt@SiO_2) were synthesized. In a typical procedure, a specific amount of platinum precursor ([$Pt(NH_3)_4(NO_3)_2$], Aladdin, Pt ≥ 50%) was dissolved in 40 mL of deionized water. After stirring for 10 min, 555.5 mg of polyvinylpyrrolidone (PVP) was added to the solution. Subsequently, 5 mL of a 0.1 mol L^{-1} $NaBH_4$ aqueous solution was added dropwise under an ice-water bath (5 °C), and the mixture was stirred for 30 min. Then, 40 mL of ethanol and 4 mL of aqueous ammonia were introduced, followed by continuous stirring at room temperature for another 30 min. Afterward, 2.55 g of tetraethyl orthosilicate (TEOS) was added into the mixture and stirred for 8 h. The volatile liquids, including ethanol and ammonia, were then removed by rotary evaporation. The resulting solid was collected in a centrifuge tube, washed with deionized water 3-5 times, and thoroughly dried at 150 °C to obtain the Pt@SiO_2 precursor. Subsequently, the obtained Pt@SiO_2 was utilized as the raw material to fabricate the Pt@zeolite catalysts via a solid-state crystallization method. Specifically, tetrapropylammonium hydroxide (TPAOH, 40 wt.%) was used as the structure-directing agent. The Pt@SiO_2 powder and TPAOH were physically mixed and uniformly ground in an agate mortar, with the molar ratio of the template to silica

meticulously controlled between 0.03 and 0.15. The homogeneously ground powder was then transferred into a Teflon-lined stainless-steel autoclave, sealed, and heated at 170 °C for 3 days to accomplish crystallization. After cooling to room temperature, the solid product was recovered by filtration, washed thoroughly with deionized water, and calcined in air at 550 °C for 2 h. Finally, the material was reduced in a 10% H_2/Ar flow at 330 °C for 3 h to yield the final Pt@zeolite catalysts. The specific Pt loading and the Si/Al atomic ratio of the catalysts were precisely tuned by adjusting the amounts of the respective precursors in the initial feed.

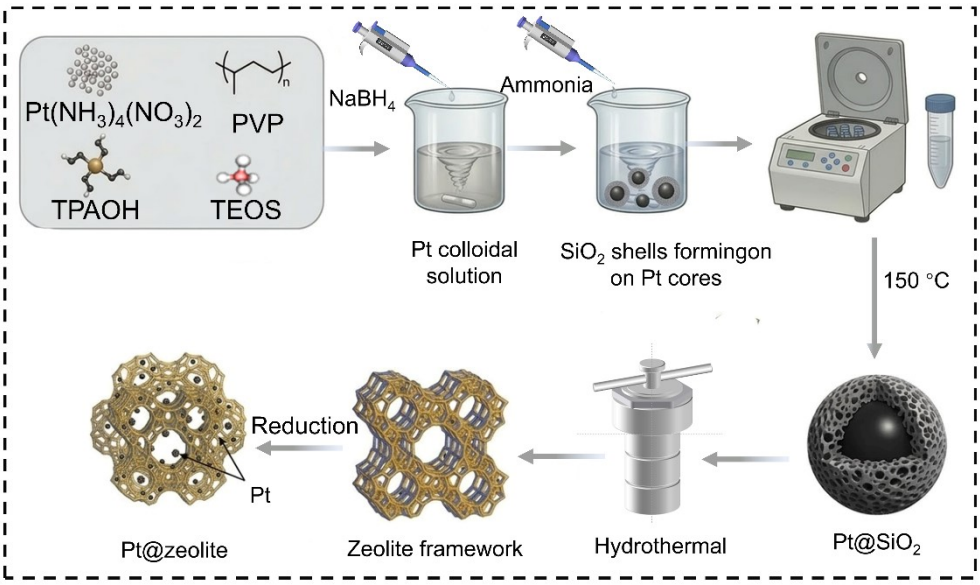

Scheme 1. Schematic illustration of the synthesis of Pt@ZSM-5 catalysts.

Synthesis of the external Pt/HZ5 control catalyst

To exclusively deposit platinum nanoparticles on the external surface of the zeolite, a template-blocking strategy was employed for the synthesis of the Pt/HZ5 control catalyst. The parent HZSM-5 zeolite was synthesized according to a modified literature protocol[2]. A structure-directing solution was prepared by mixing 8.12 g of potassium-free tetrapropylammonium hydroxide solution with a mass fraction of 40% and 20.1 g of distilled water at room temperature. Tetraethyl orthosilicate weighing 8.24 g was

introduced into this basic mixture to undergo complete hydrolysis under a constant stirring speed of 500 revolutions per minute for 6 hours. The resulting homogeneous gel was transferred into a Teflon-lined stainless-steel autoclave and heated in an electric oven at 175 °C for 96 hours under static conditions. The solid product was isolated by filtration and washed thoroughly with copious amounts of distilled water and acetone before drying at 60 °C. To strictly confine the subsequent metal deposition to the exterior, this as-synthesized zeolite was deliberately utilized as the catalytic support without any prior calcination. The intact organic template effectively occupied the intrinsic micropores. This physical blockage of the internal void space ensured that the platinum precursor introduced via conventional wet-impregnation was forced to deposit exclusively on the outer surface of the zeolite crystals. The impregnated material was finally subjected to sequential calcination and reduction treatments to simultaneously eliminate the internal organic template and activate the external platinum nanoparticles.

Catalyst Structural Analysis and Characterization

Powder X-ray diffraction (XRD) patterns were recorded on a Bruker D8 Discover diffractometer equipped with a monochromatic Cu Kα radiation source. The scans were collected in the 2θ range of 10-70° with a step size of 0.03°. The morphological and structural features of the catalysts were examined using a Talos F200S transmission electron microscope (TEM) operated at an accelerating voltage of 200 kV. The textural properties of the samples were evaluated by N_2 adsorption–desorption isotherms at 77 K using a Micromeritics ASAP 2460 surface area and porosity analyzer. Prior to the measurements, the samples were degassed under dynamic vacuum at 573 K for 6 h to exhaustively remove moisture and strongly adsorbed impurities residing in the porous

network. The specific surface area was determined utilizing the Brunauer-Emmett-Teller (BET) method.

All infrared spectroscopic data were acquired on a PerkinElmer Frontier spectrometer equipped with a liquid-nitrogen-cooled MCT detector and a custom-built, high-vacuum *in-situ* transmission cell. The spectra were collected with a resolution of 4 cm^{-1} and an accumulation of 64 scans per spectrum.

(a) Quantitative assessment of surface acidity via Py-IR:

The catalyst powder was pressed into a self-supporting wafer and pretreated by annealing at 573 K under dynamic vacuum (~10^{-4} Pa) for 2 h. Upon cooling to 353 K, pyridine vapor was introduced into the cell until adsorption saturation was reached, followed by evacuation for 30 min to completely eliminate physically adsorbed pyridine species. The absolute concentrations of Brønsted and Lewis acid sites were quantified based on the integrated areas of their characteristic bands at 1545 cm^{-1} and 1455 cm^{-1}, respectively. The quantification was performed applying the Beer-Lambert law, taking into account the wafer mass, cross-sectional area, and established molar extinction coefficients[3].

(b) Dynamic adsorption and isotopic exchange of probe molecules:

To elucidate the surface interactions between the catalysts and specific probe molecules (D_2, H_2O, and CO), the self-supporting wafer was first reduced *in-situ* at 573 K in an H_2 flow for 30 min, and subsequently annealed under high vacuum for 2 h to ensure a rigorously clean surface. After cooling to 353 K, the purified probe gases or

vapors were precisely dosed into the cell via a high-precision leak valve for dynamic spectral acquisition.

Catalytic Performance Evaluation

The catalytic performance for the gas-phase hydrogen-water isotopic exchange reaction was evaluated using a continuous-flow fixed-bed reactor at atmospheric pressure as shown in Figure S4. We varied the total gas flow rate while keeping the space velocity constant. The specific reaction rate remained perfectly constant across different flow rates, unequivocally confirming the absence of external film diffusion limitations. Prior to the catalytic tests, the catalyst powder was pelletized, crushed, and sieved to a uniform particle size of 40-60 mesh. To rigorously exclude potential internal/external mass transport limitations and thermal gradients during the reaction, the catalyst granules were homogeneously diluted with purified, inert quartz sand. Before each evaluation run, the catalyst was subjected to an *in-situ* reduction process in a stream of 20 vol% H_2/Ar at 573 K for 1 h, applying a controlled heating rate of 5 K/min. Upon cooling the system to the designated reaction temperature, the catalytic reaction was initiated by introducing a reactant gas mixture (80 vol% H_2/Ar) co-fed with deuterated water vapor. Specifically, the deuterated water vapor was continuously generated by delivering a 20 wt.% HDO aqueous solution into an upstream preheating zone via a high-precision micro-syringe pump, ensuring complete vaporization prior to reaching the catalyst bed. The total gas flow rate was precisely regulated by mass flow controllers to maintain a constant gas hourly space velocity (GHSV) of 6×10^6 mL·gcat^{-1}·h^{-1}.

Density Functional Theory and Computational Modeling

All first-principles theoretical simulations were executed utilizing the Vienna *ab initio* simulation package (VASP, version 6.3.0)[4]. To precisely describe the electron exchange-correlation interactions, the generalized gradient approximation (GGA) parameterized by the Perdew-Burke-Ernzerhof (PBE) functional was adopted[5]. The ion-electron interactions were modeled via the projector-augmented wave (PAW) pseudopotentials, coupled with a plane-wave basis set truncated at a kinetic energy of 500 eV. Geometry optimizations were considered converged once the maximal residual forces on individual atoms dropped below 0.03 eV $Å^{-1}$. Furthermore, unrestricted spin-polarization was enabled globally, and the semi-empirical Grimme's DFT-D3 scheme equipped with Becke-Johnson (BJ) damping was incorporated to accurately capture the long-range van der Waals dispersion forces. The minimum energy pathways and the precise locations of transition states (TSs) were rigorously identified employing the climbing image nudged elastic band (CI-NEB) method. Subsequent vibrational analyses, computed by finite displacements, confirmed the physical validity of these TSs (characterized by a single imaginary frequency) and provided the necessary zero-point energy (ZPE) corrections for all stationary points.

For the geometric model, the reciprocal space was sampled utilizing a 1 × 1 × 2 Monkhorst–Pack *k*-point mesh. The fully relaxed lattice constants of the ZSM-5 framework (a = 19.92 Å, b = 19.94 Å, c = 13.29 Å) exhibited excellent consistency with empirical crystallographic data[6]. To construct the active microenvironment (denoted as Pt_4@HZSM-5), a specific crystallographic T4-site silicon atom was

isomorphously substituted by an aluminum atom[7, 8]. The resultant framework negative charge was compensated by an H^+ cation (forming a Brønsted acid site), adjacent to which a sub-nanometric Pt_4 cluster was anchored near the $[AlO_4]^-$ tetrahedron, collectively serving as the reactive center. Mimicking the authentic *in operando* catalytic conditions, the metallic Pt_4 ensemble was pre-covered by eight dissociated hydrogen atoms. During the mechanistic tracking of the direct exchange, the initial configuration was intentionally designed by localizing an atomic H on the Pt site closest to the H^+, while a discrete HDO molecule was adsorbed onto the neighboring Brønsted acid site. This specifically tailored structural model profoundly enables the atomistic decryption of the fundamental H_2-HDO exchange pathways.

It should be noted that the present DFT simulations employ a simplified Pt_4 cluster near a single Al/BAS configuration, whereas the experimental catalysts feature ~4 nm Pt nanoparticles and randomly distributed Al T-sites. While this model simplifies the geometric complexity of the realistic metal-support interface, the core mechanistic conclusions are expected to remain robust. Experimentally, Our previous research showed that H_2-HDO exchange exhibits the characteristics of a structurally insensitive reaction[9], where the intrinsic turnover frequency is largely independent of the Pt particle size, justifying the use of a sub-nanometer cluster to capture the localized interfacial electron transfer. More importantly, the sensitivity of the spillover barrier to the exact Pt-BAS physical distance or specific Al siting is essentially leveled out by the extended hydrogen-bonded water networks. Under reaction conditions, multiple water molecules assemble into oligomeric chains within the micropores, acting as a highly efficient

proton highway with an exceptionally low proton-hopping barrier. These dynamic water bridges can effectively wire the remote BAS to the Pt surface, rendering the energetically favorable interfacial hydrogen transfer universally viable across diverse and realistic zeolitic configurations.

Table S1: Analysis of Pt metal content, specific surface area and acidity of different catalysts.

Sample	S_{BET} (m^2 g^{-1})	Pt content[a] %	Pyridine adsorption		E_a kJ/mol
			C_B (μmol g^{-1})	C_L (μmol g^{-1})	
HZSM-5-200	410.2	-	103.3	22.0	-
0.1Pt@HZ5-200	389.9	0.11	100.5	21.0	25.8
0.4Pt@HZ5-200	382.5	0.42	103.5	22.4	24.9
0.6Pt@HZ5-200	380.8	0.60	103.0	23.1	21.6
0.8Pt@HZ5-200	370.6	0.82	104.0	23.5	24.6
0.4Pt@HZ5-40	-	-	219.3	95.2	-
0.4Pt@HZ5-100	-		190.4	57.0	-
0.4Pt@HZ5-150	-	-	126.3	42.3	-
0.4Pt@HZ5-200	-	-	103.5	22.4	-
0.4Pt@NaZ5-200		0.41	0	143.0	36.0
0.4Pt@ Silicalite-1		0.40	10.1	56.8	34.0
Pt/C	-	20	-	-	63.6

[a] Determined by ICP-OES.

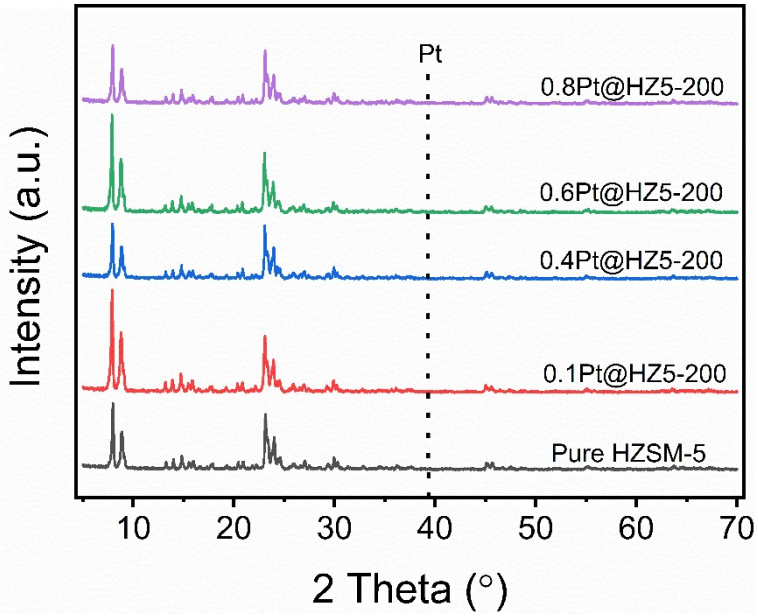

Figure S1. XRD patterns of different catalysts.

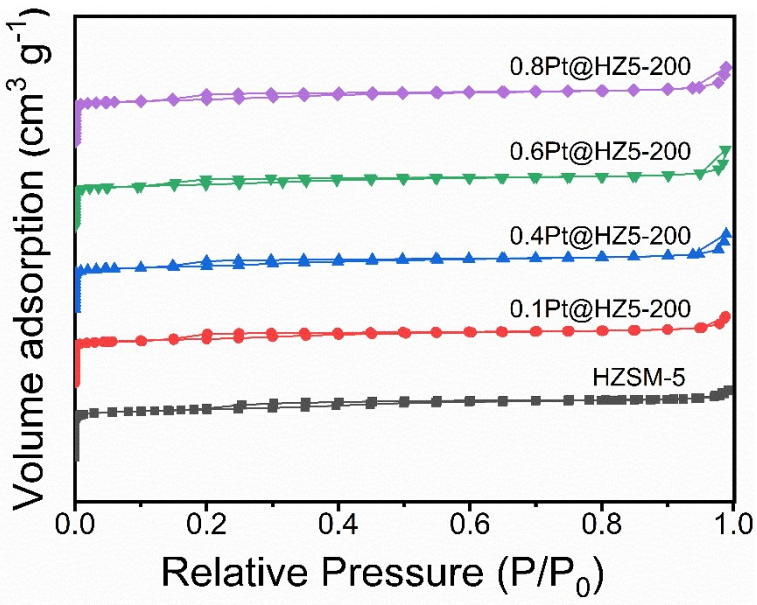

Figure S2. N_2 adsorption-desorption isotherms of different samples

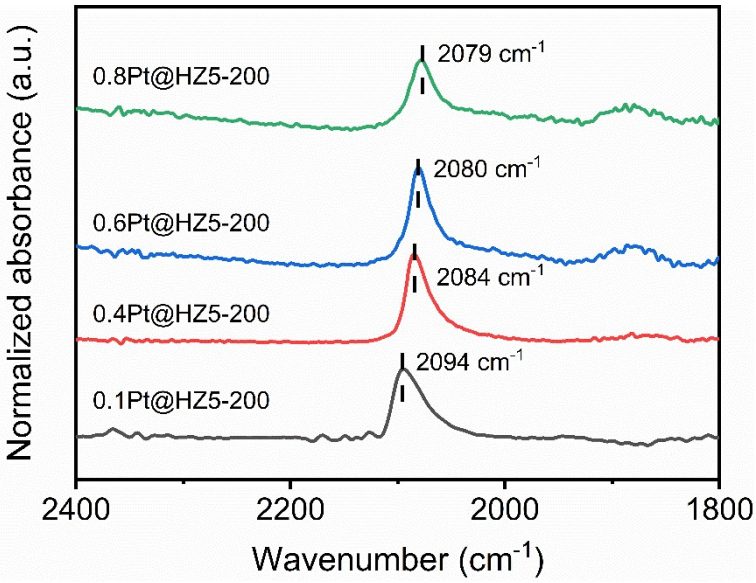

Figure S3. In-situ CO adsorbed FTIR spectra of different catalysis.

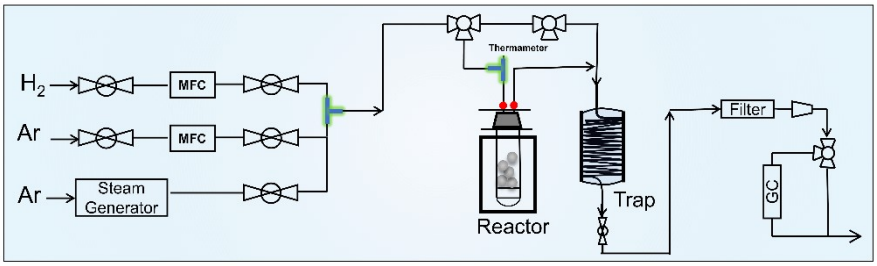

Figure S4. Schematic diagram of a fixed-bed reactor for gas-phase hydrogen-water isotopic catalytic exchange.

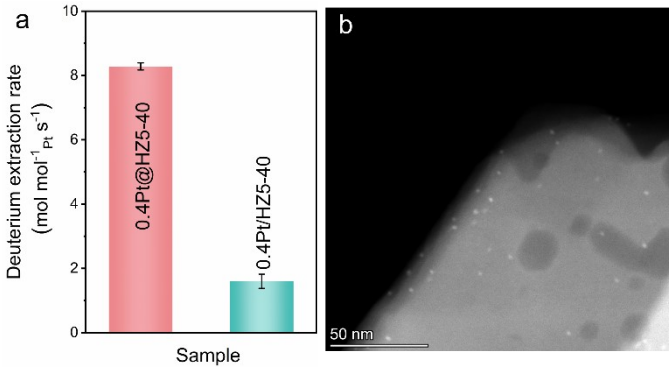

Figure S5. (a) Catalytic evaluation for deuterium extraction on Pt@HZ5 and Pt/HZ5 catalysts, (b) STE M of the Pt/HZ5 catalysts.

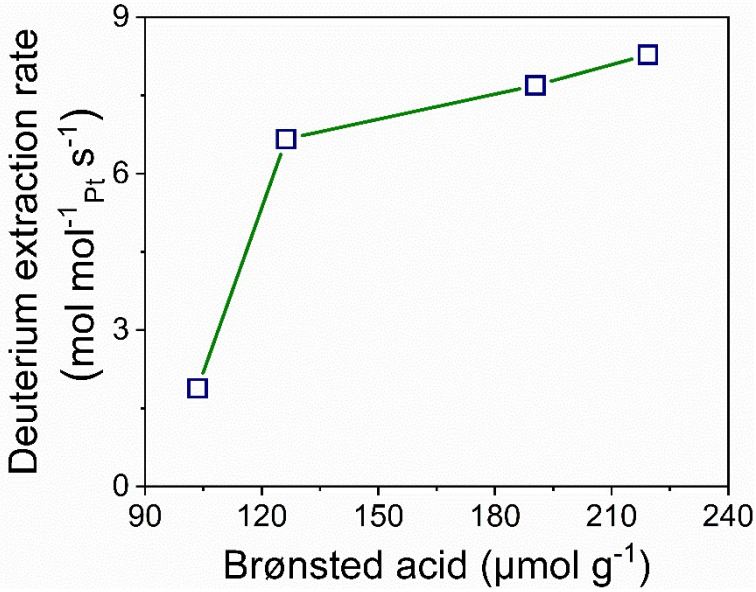

Figure S6. Correlation between the Brønsted acid site density and the intrinsic hydrogen isotope exchange rate.

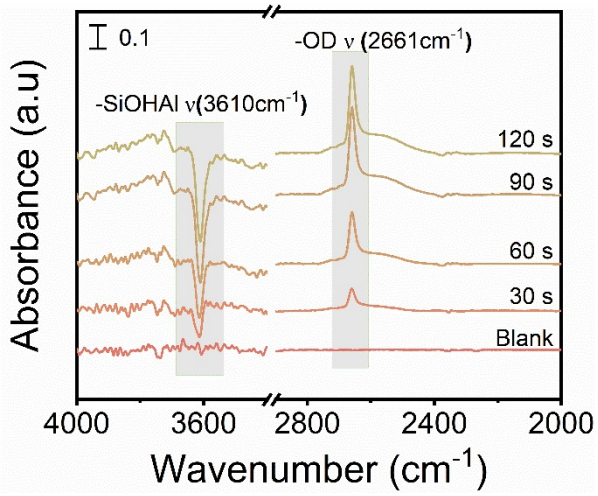

Figure S7. Time profiles of the integrated FT-IR peak areas for the Si-OH-Al (3610 cm^{-1}) and Si-OD-Al (2661 cm^{-1}) stretching vibrations during the D_2 adsorption process over the Pt@HZ5 catalyst.

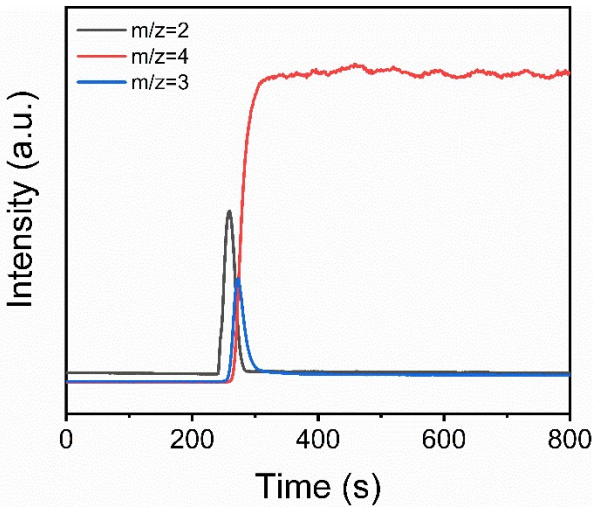

Figure S8. Time-resolved mass spectrometry (MS) profiles of H_2, HD, and D_2 during the transient D_2 isotope exchange process over the vacuum-annealed Pt@HZ5 catalyst. The rapid emergence of HD and H_2 signals immediately upon D_2 introduction highlights the ultra-fast dissociation of D_2 on the Pt surface and the subsequent spillover-driven exchange with the intrinsic protons of the Brønsted acid sites.

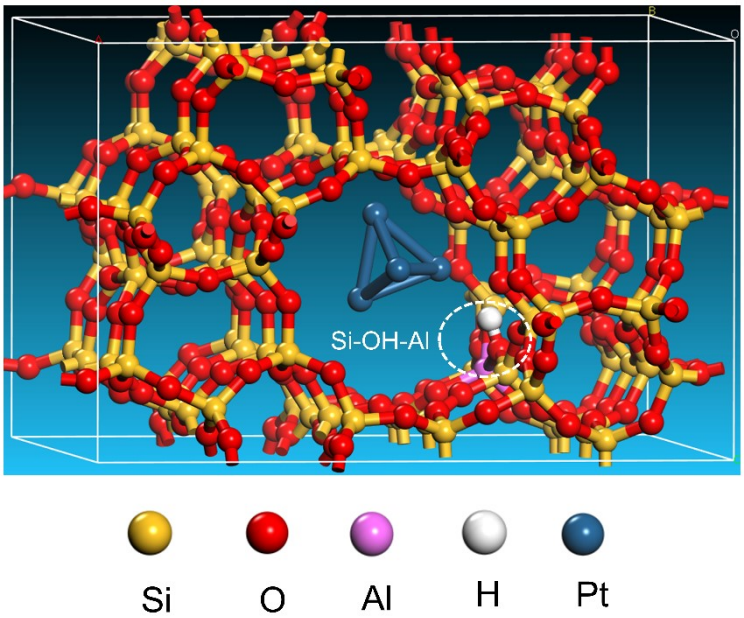

Figure S9. Optimized geometric models of Pt@HZ5.

REFERENCES

1. Z. Jin, L. Wang, E. Zuidema, K. Mondal, M. Zhang, J. Zhang, C. Wang, X. Meng, H. Yang, C. Mesters and F. S. Xiao, *Science*, 2020, **367**, 193-197.
2. L. Liu, M. Lopez-Haro, C. W. Lopes, C. Li, P. Concepcion, L. Simonelli, J. J. Calvino and A. Corma, *Nat. Mater.*, 2019, **18**, 866-873.
3. C. A. Emeis, *J. Catal.*, 1993, **141**, 347-354.
4. G. Kresse and J. Hafner, *Phys. Rev. B*, 1993, **48**, 13115-13118.
5. J. P. Perdew, K. Burke and M. Ernzerhof, *Phys. Rev. Lett.*, 1996, **77**, 3865-3868.
6. G. T. Kokotailo, S. L. Lawton, D. H. Olson and W. M. Meier, *Nature*, 1978, **272**, 437-438.
7. K. Sun, F. Fan, H. Xia, Z. Feng, W.-X. Li and C. Li, *The Journal of Physical Chemistry C*, 2008, **112**, 16036-16041.
8. E. N. Domoroshchina, R. D. Svetogorov, G. M. Kuz'micheva, G. V. Kravchenko, L. V. Pirutko, A. I. Zhukova, A. N. Utenyshev and K. V. Bozhenko, *Journal of Materials Science*, 2023, **58**, 3934-3946.
9. H. Wang, Y. Yang, S. Yu, B. Zhang, J. Xie, J. Chen, D. Wang, B. Feng, C. Zhong, L. Zhou, W. Cui, D. Ma and Y. Yao, *J. Catal.*, 2024, **430**, 115345.